

The Energetics of Li Off-Centering in $K_{1-x}Li_xTaO_3$: First Principles Calculations

S. A. Prosandeev^{1,2}, E. Cockayne¹, and B. P. Burton¹

¹*Ceramics Division, Materials Science and Engineering Laboratory,*

National Institute of Standards and Technology, Gaithersburg, Maryland 20899-8520

²*Physics Department, Rostov State University, 5 Zorge St., 344090 Rostov on Don, Russia*

(Dated: March 27, 2018)

$K_{1-x}Li_xTaO_3$ (KLT) solid solutions exhibit a variety of interesting physical phenomena related to large displacements of Li-ions from ideal perovskite A-site positions. First-principles calculations for KLT supercells were used to investigate these phenomena. Lattice dynamics calculations for KLT exhibit a Li off-centering instability. The energetics of Li-displacements for isolated Li-ions and for Li-Li pairs up to 4th neighbors were calculated. Interactions between nearest neighbor Li-ions, in a Li-Li pair, strongly favor ferroelectric alignment along the pair axis. Such Li-Li pairs can be considered “seeds” for polar nanoclusters in KLT. Electrostriction, local oxygen relaxation, coupling to the KT soft-mode, and interactions with neighboring Li-ions all enhance the polarization from Li off-centering. Calculated hopping barriers for isolated Li-ions and for nearest neighbor Li-Li pairs are in good agreement with Arrhenius fits to experimental dielectric data.

I. INTRODUCTION

Potassium tantalate, $KTaO_3$ (KT), is a cubic perovskite with a quantum paraelectric ground state.¹ In $K_{1-x}Li_xTaO_3$ (KLT) solid solutions, Li-ions substitute for K on perovskite A-sites. Li-ions are smaller than K, and displace from ideal, centrosymmetric, A-sites by about 1.26 Å along cubic $[0,0,1]$ -type vectors $([0,0,1]_c)$.² Displacements of Li-ions generate strong local dipole moments [Li-dipole(s)] which couple electrostatically to the KT polar soft-mode. Near neighbor (nn) Li-dipoles can also interact to form polar nanoclusters (PNC); i.e. multicell regions in which the local polarization direction is strongly correlated. The complex nature of ferroelectric (FE) ordering in KLT derives from a combination of interactions between Li-dipoles, the soft-mode, and PNC.

In the composition range $0 < x < 0.02$, KLT is a quantum paraelectric, but for $0.02 < x < 0.06$, both FE and dipole-glass characteristics are observed.^{3,4,5} In the temperature (T) interval $0 < T \lesssim 100$ K, the dielectric permittivity, $\epsilon(T)$, has a peak, and second harmonic generation exhibits an abrupt increase, with hysteresis.^{6,7} The existence of randomly distributed and randomly poled PNC was established from dielectric measurements, birefringence and nuclear magnetic resonance (NMR).^{3,5,8,9} Neighboring PNC may touch, but PNC-coarsening is apparently prevented by random long-range PNC-PNC interactions.⁷ In zero applied field, a glassy phase is observed,⁵ however, a sufficient applied field will induce FE long-range order (LRO).^{3,5,6} For $0.06 \lesssim x < 0.15$, KLT undergoes a FE phase transition at $T \gtrsim 100$ K, even in the absence of an applied field. At $x > 0.15$, the perovskite solid solution is no longer stable.

Dielectric measurements on KLT with $0 < x < 0.02$ exhibit only one relaxational peak in $\epsilon(T)$, while at $x \approx 0.04$, two peaks are observed, and they are associated with two relaxational processes (fast and slow).^{8,10,11,12} Temperature variations of both relaxation processes follow Arrhenius laws; $\tau \sim \tau_0 e^{-U/kT}$. The fast process activation energy is $U \approx 1000$ K (86 meV), and the slow pro-

cess, at $0.02 < x < 0.06$, has been reported as 2100 K,¹³ 2400 K,¹¹ and 2800 K.¹²

The fast process 1000 K activation energy is believed to be the barrier for an isolated Li-ion to hop from one $[0,0,1]_c$ position to another separated by a 90° angle. NMR data support this hypothesis.² The slow process with an activation energy of $2100 \lesssim U \lesssim 2800$ K^{11,12,13} is less well understood. On the basis of acoustic measurements it was hypothesized^{8,10} that the slow process might be 180° correlated Li-Li nn pair reorientations (e.g. $z - z \rightleftharpoons \bar{z} - \bar{z}$ relaxation for nn separated by $a_0 \hat{z}$ where a_0 is the lattice parameter of the primitive cubic unit cell, and \hat{z} is a unit vector in the $[0,0,z]$ direction).

The energy spectrum and kinetics of PNC reorientation is a general problem for FE systems that exhibit both relaxor and soft-mode behavior (cf.¹⁴). KLT is a relatively simple model system for such phenomena because isolated Li-ions in KLT solutions can be regarded as randomly distributed sources of 6-state Potts-like dipole fields.^{15,16,17} Previous modeling of KLT includes: Semi-empirical shell model calculations¹⁸; Intermediate neglect of the differential overlap (INDO) calculations^{19,20}; Full potential linear muffin-tin orbital (FPLMTO) calculations^{20,21} (without ionic relaxations). All these studies yielded potential barriers for 90° Li-hopping that were significantly lower than those deduced from experimental fits.

KLT solutions with $0.016 < x < 0.05$ exhibit a large photocurrent below 80K.^{22,23,24} No photocurrent has been observed in pure KT, nor in solid solutions of KT with $KNbO_3$. Photocurrent is usually thought to be associated with O-hole centers near Li-occupied A-sites²². Recent INDO calculations²⁰ confirmed that displacements of O^{2-} -ions which are nn of Li create shallow states in the forbidden gap.

First-principles (FP) computations allow determinations of the electronic structures and energetics as functions of ionic coordinates, and thus provide a sound basis for understanding and quantitatively modeling KLT. In this work, FP density functional theory (DFT) methods

were used to calculate the energetics of Li off-centering for isolated Li-ions, and for Li-Li pairs up to fourth neighbors. The energetics of 90° isolated Li-ion hopping and 180° Li-Li nn-pair hopping were calculated. Lattice dynamics studies of KLT demonstrate correlated motions of Li and the surrounding ions (particularly nn O^{2-}). Total polarization from Li off-centering, and individual contributions from different ions were quantified. Electronic band structures were calculated to investigate shallow electronic states that may promote photocurrent.

II. METHODS

All DFT calculations were done with the Vienna *ab initio* simulation package (VASP)^{25,26}. A plane wave basis set for electronic wavefunctions and ultrasoft pseudopotentials were used²⁷ in the local density approximation (LDA) for exchange and correlation energies. VASP computes interatomic forces and total energies for crystals, and allows either global or constrained relaxations of internal coordinates and/or lattice parameters. Frozen-phonon methods were used to obtain force constants for computing lattice dynamics. Berry phase analyses, as implemented in VASP by M. Marsman, were used to calculate dynamical charges.

Investigating the effects of Li-ions in KLT with low Li concentration requires large supercells, *e.g.* (Fig. 1): (a) KT40, a 40 atom supercell of pure $KTaO_3$; (b) KLT40, a 40 atom supercell with basis vectors $[0, 0, 2]_c$, $[0, 2, 0]_c$ and $[2, 0, 0]_c$ (units of a_0 , $x = 0.125$); (c) KLT80a an 80 atom supercell with basis vectors $[2, 2, 0]_c$, $[2, 0, 2]_c$, and $[0, 2, 2]_c$ and $x = 0.0625$; (d) KLT80b, same as KLT80a but with two Li per supercell, $x = 0.125$, separated by $a_0\hat{z}$; (e, f, g) KLT80c, KLT80d, KLT80e, same as KLT80b, but with two Li separated by $a_0(\hat{x} + \hat{y})$, $a_0(\hat{x} + \hat{y} + \hat{z})$ and $2a_0\hat{z}$, respectively. For KT40 and KLT40, a $4 \times 4 \times 4$ Monkhorst-Pack k -point grid was used and for KLT80a, etc., a $2 \times 2 \times 2$ grid. Results for KLT80a are negligibly different with a $4 \times 4 \times 4$ Monkhorst-Pack grid.

This computational scheme was tested on pure KT with 5 atoms per cell. The VASP lattice constant $a = 3.96$ Å agrees with previous LDA computations²⁸, and is smaller than the experimental values (between 3.987 Å and 3.989 Å at room temperature^{1,29,30,31}). The calculated bulk modulus for a KT40 supercell with $4 \times 4 \times 4$ k -point grid is 2.0 Mbar, which is lower than the experimental¹ value 2.3 Mbar. A first principles LDA result for a 5-ion primitive cell with an $8 \times 8 \times 8$ k -point grid is 2.1 Mbar²⁸, but a full-potential linear muffin-tin orbital calculation, primitive cell and $8 \times 8 \times 8$ k -point grid yielded,³² 2.3 Mbar. Hence, ultrasoft pseudopotentials provide reasonable accuracy compared with other *ab initio* calculations.

III. RESULTS

A. Reference Structures

To study Li off-centering, one needs a reference structure in which Li occupies an ideal centrosymmetric A-site. A 40-atom reference structure, KLT40_{Ref}, is obtained by placing all ions of KLT40 on ideal perovskite positions and optimizing lattice parameters and internal coordinates (except Li), subject to a cubic symmetry constraint. The resulting cell has $a = 2 \times 3.956$ Å. Crystallographic data for KLT40_{Ref}, are tabulated in Table I. Because Li is smaller than K, there is a volume contraction around Li such that nn Ta ions displace by 0.010 Å towards Li, and nn O ions displace by 0.024 Å towards Li.

TABLE I: Calculated structure for KLT40_{Ref}:KLT40 with Li occupying ideal A-site positions, and the structure relaxed, subject to a cubic symmetry constraint. Space group $Pm\bar{3}m$; $a = 2 \times 3.9559$ Å.

ion	Wyckoff position	x	y	z
K ₁	1a	0.0000	0.0000	0.0000
K ₂	3d	0.0000	0.0000	0.5000
K ₃	3c	0.5000	0.5000	0.0000
Li	1b	0.5000	0.5000	0.5000
Ta	8g	0.2508	0.2508	0.2508
O ₁	12i	0.2509	0.2509	0.0000
O ₂	12j	0.2522	0.2522	0.5000

A series of KLT40_{Ref} frozen phonon calculations, with each symmetry-independent ion displaced in turn, was used to compute force constants, construct the dynamical matrix, and compute zone-center normal mode frequencies and eigenvectors. Symmetry analysis of KLT40_{Ref} zone-center phonons yields $3A_{1g} + 2A_{2g} + 3A_{2u} + 5E_g + 3E_u + 5F_{1g} + 14F_{1u} + 6F_{2g} + 7F_{2u}$. Normal mode frequencies are listed in Table II. One zone-center instability is found for KLT40_{Ref}, with symmetry F_{1u} . Thus, as expected, the high-symmetry reference structure is dynamically unstable. Table III, gives the F_{1u} instability eigenvector, which is dominated by a Li off-centering $[0, 0, d]_c$ displacement.

For comparison, the force constants of a 40-atom cell of pure $KTaO_3$ (KT40) were calculated at the same lattice parameter. The TO normal mode results are listed in Table IV. Force constants for KT40 and KLT40_{Ref} are nearly identical. The only interatomic force constants that change by more than 0.41 eV/Å² are those involving the 12 O-ions that are nn of Li. For example, the radial interionic force constant between an A-ion and a nn-O changes sign from -0.21 eV/Å² in KT to $+0.74$ eV/Å² in KLT40_{Ref} when K is replaced by Li. The positive sign for this term in KLT40_{Ref} implies that Li-motion in opposition to its nn O-ions is energetically favorable. Thus, the single lattice instability in KLT40_{Ref} is dominated by Li-motion (85% of the dynamical matrix eigen-

TABLE II: Computed zone-center normal mode symmetries and frequencies (ν in cm^{-1}) for KLT40_{Ref} (Table I). F_{1u} frequencies are for transverse optical modes, except for the zero-frequency acoustic triplet. Also listed are relative amplitudes a_{rel} for each mode in the fully relaxed tetragonal KLT40 structure. The relaxation is dominated by the eigenvector of the 172 i cm^{-1} instability. In addition to the ferroelectric distortion itself which has F_{1u} symmetry, there are secondary distortions of A_{1g} - and E_g -type.

symm.	ν	a_{rel}	symm.	ν	a_{rel}	symm.	ν	a_{rel}
A_{1g}	211	0.0906	F_{1g}	70	0.0000	F_{2g}	63	0.0000
A_{1g}	418	0.0877	F_{1g}	205	0.0000	F_{2g}	178	0.0000
A_{1g}	445	0.0504	F_{1g}	338	0.0000	F_{2g}	262	0.0000
			F_{1g}	527	0.0000	F_{2g}	327	0.0000
A_{2g}	167	0.0000	F_{1g}	611	0.0000	F_{2g}	534	0.0000
A_{2g}	285	0.0000				F_{2g}	910	0.0000
			F_{1u}	172 i	2.9599			
A_{2u}	58	0.0000	F_{1u}	0	0.0000	F_{2u}	129	0.0000
A_{2u}	507	0.0000	F_{1u}	120	0.3047	F_{2u}	159	0.0000
A_{2u}	945	0.0000	F_{1u}	164	0.0596	F_{2u}	178	0.0000
			F_{1u}	177	0.0080	F_{2u}	243	0.0000
E_g	125	0.6230	F_{1u}	187	0.2049	F_{2u}	256	0.0000
E_g	213	0.1954	F_{1u}	200	0.0082	F_{2u}	331	0.0000
E_g	279	0.2125	F_{1u}	205	0.2038	F_{2u}	349	0.0000
E_g	422	0.1413	F_{1u}	244	0.0961			
E_g	448	0.1241	F_{1u}	336	0.0901			
			F_{1u}	364	0.0041			
E_u	69	0.0000	F_{1u}	432	0.0373			
E_u	495	0.0000	F_{1u}	555	0.0378			
E_u	577	0.0000	F_{1u}	862	0.0075			

TABLE III: Dynamical matrix eigenvector for the z -polarized 172 i cm^{-1} mode. Ionic labels correspond to those in table I.

ion	x	y	z	e_x	e_y	e_z
K ₁	0.0000	0.0000	0.0000	0.0000	0.0000	0.0206
K ₂	0.0000	0.0000	5.0000	0.0000	0.0000	-0.0374
K ₂	0.5000	0.0000	0.0000	0.0000	0.0000	0.0036
K ₃	0.5000	0.5000	0.0000	0.0000	0.0000	0.0507
K ₃	0.0000	0.5000	0.5000	0.0000	0.0000	-0.0350
Li	0.5000	0.5000	0.5000	0.0000	0.0000	0.9252
Ta	0.2508	0.2508	0.2508	0.0300	0.0300	0.0252
O ₁	0.2509	0.2509	0.0000	0.0000	0.0000	-0.0509
O ₁	0.0000	0.2509	0.2509	-0.0187	0.0000	-0.0301
O ₂	0.2522	0.2522	0.5000	0.0000	0.0000	-0.0242
O ₂	0.5000	0.2522	0.2522	0.0000	-0.0649	-0.0875

vector) opposite its nn O (12% of the dynamical matrix eigenvector). Because KLT40_{Ref} and KT40 have such similar force constant matrices, their normal mode spectra are very similar. Note that each TO mode in KT40 has a corresponding TO mode of very similar frequency in KLT40_{Ref}.³³

TABLE IV: Computed TO normal mode frequencies (ν in cm^{-1}) and dynamical matrix eigenvectors for KTaO₃ at $a = 3.956$ Å.

ν	u_K	u_{Ta}	$u_{O\parallel}$	$u_{O\perp}$
115	-0.2989	0.5419	-0.3937	-0.4807
205	0.8745	-0.1737	-0.2401	-0.2715
555	0.0012	0.0341	-0.8531	0.3682

B. Fully Relaxed Structures

Full ionic relaxation in KLT40 indicates that (consistent with previous unrelaxed computations^{20,21}) maximum energy reduction occurs when Li-ions are displaced to $[0, 0, d]_c$ (Figs. 2-3). The calculated equilibrium Li-displacement³⁴ is $d=1.009$ Å (Table V), whereas fits to experimental data yield² $d = 1.26$ Å. For comparison, the curves obtained when all ions, except for Li, are fixed at ideal perovskite positions, are also shown in Fig. 3. Clearly, the depth of the well and the magnitude of Li-displacement are sensitive to relaxations of the surrounding ions, consistent with earlier results.¹⁹

The largest sympathetic distortion associated with Li-displacements involve four nn O-ions (see Table V and Fig. 2), which are displaced towards Li by 0.109 Å. Similar correlated Li- and O-displacements occur in LiNbO₃ and LiTaO₃³⁵. In each case, as Li displaces, the oxygen atoms that Li approaches move toward the Li, and those left behind back away, as might be expected from electrostatics. The magnitude of Li displacement is about 0.3 Å in LiTaO₃³⁵ or 0.4 Å with full geometry optimization,³⁶ i.e., much smaller than Li in KLT. Note, however, that LiTaO₃ and LiNbO₃ have the LiNbO₃ structure type, a derivative of the corundum structure, not the perovskite type, and that the displacements patterns are therefore not directly comparable.

The results listed in Table V indicate that Ta-ions are generally displaced in the same direction as Li, while O-ions shift in the opposite direction. This is consistent with the view that Li-displacement leads to freezing of a soft-mode polarization fluctuation that has a large correlation radius.

A breakdown of the displacement pattern into normal mode coordinates for KLT40_{Ref} is shown in Table II. Anharmonic coupling leads to some contributions from higher frequency modes, but otherwise, the displacement pattern is dominated by the eigenvector of the structural instability. Vibrational frequencies for fully relaxed KLT40 were also calculated, and symmetry analysis of the fully relaxed tetragonal structure indicates that the phonon spectrum is $22 A_1 + 8A_2 + 14B_1 + 12B_2 + 32E$. Modes belonging to irreducible representations A_1 and E are infrared active (except for the $A_1 + E$ acoustic set). The frequencies of infrared active modes are listed in Tables VI. Each column represents the (summed) projection (in percent) of the dynamical matrix eigenvector of relaxed KLT40 onto one (or more) eigenvectors of

KLT40_{Ref.}. If two eigenvectors were identical, the entry would be 100.

The KT soft-mode frequency (at equilibrium lattice constant), 120 cm⁻¹, splits into two modes in fully relaxed KLT40: E (124 cm⁻¹), and A_1 (163 cm⁻¹). Hence, the averaged frequency for these modes is increased by Li-displacement as indicated by experimental data for hardening of the soft-mode in KLT³⁷. However, calculated hardening of the soft mode is only significant for the component of the KT soft-mode triplet that is polarized in the Li-displacement direction.

To study x -dependence of the soft mode splitting, lattice dynamics were calculated for KT4O ($x = 0$), KLT80a ($x = 0.0625$), and KLT40 ($x = 0.125$), all with fixed $a = 3.9879\text{\AA}$ (the experimental value³¹ for $x = 0.05$). Results for the soft mode splitting are shown in Table VII. The calculated splitting increases with x . TO splitting in the ferroelectric phase of KLT has been observed experimentally by Raman spectroscopy³⁸ and by neutron scattering³⁹. The measured splitting³⁹ in tetragonal KLT with $x = 0.05$ is given in Table VII. The experimental splitting is less than that obtained from FP results, owing to the use of periodic boundary conditions in FP calculations, which fixes the arrangement of the Li-sites and artificially aligns Li-dipoles from one supercell to the next (cf. Ref. [40]).

The Li-dominated instability of KLT40_{Ref.} mixes with several other modes; its weighted average frequency is about 260 cm⁻¹ in the polar direction and 330 cm⁻¹ in transverse directions.

To investigate the Li-isotope effect in KLT, phonon frequencies in Table VI were recalculated using ⁶Li ($m = 6.015$ amu) instead of natural Li ($m = 6.941$ amu). Individual mode frequencies increase when ⁶Li is used,

TABLE V: Computed fully relaxed structure of KLT40. Space group P4mm; $a = 2 \times 3.9565$ Å; $c = 2 \times 3.9638$ Å; $c/a \approx 1.002$. Deviations are relative to positions in KLT40_{Ref.}. The origin is chosen so that both structures have the same center of mass. Wyckoff positions (pos.) are used.

ion	pos.	x	y	z	δx , Å	δy , Å	δz , Å
K ₁	1a	0.0000	0.0000	0.0014	0.000	0.000	0.011
K ₂	2c	0.5000	0.0000	0.9996	0.000	0.000	-0.003
K ₃	2c	0.5000	0.0000	0.4963	0.000	0.000	-0.029
K ₄	1a	0.0000	0.0000	0.4952	0.000	0.000	-0.038
K ₅	1b	0.5000	0.5000	0.0074	0.000	0.000	0.058
Li	1b	0.5000	0.5000	0.6273	0.000	0.000	1.009
Ta ₁	4d	0.2513	0.2513	0.2526	0.004	0.004	0.015
Ta ₂	4d	0.2494	0.2494	0.7499	-0.011	-0.011	0.005
O ₁	4d	0.2515	0.2515	0.9935	0.005	0.005	-0.051
O ₂	4d	0.2474	0.2474	0.4957	-0.038	-0.038	-0.034
O ₃	4e	0.0000	0.2500	0.2436	0.000	-0.007	-0.058
O ₄	4e	0.0000	0.2533	0.7457	0.000	0.019	-0.027
O ₅	4f	0.5000	0.2482	0.2442	0.000	-0.031	-0.063
O ₆	4f	0.5000	0.2589	0.7379	0.000	0.053	-0.079

TABLE VI: Computed TO normal mode frequencies (ν in cm⁻¹) for modes of symmetry E (left) and A_1 (right) in fully relaxed KLT40. Also shown is the squared projection (in percent) of the eigenvector of each mode onto an eigenvector, or set of eigenvectors, of the dynamical matrix for KLT40_{Ref.} (1) The 172i cm⁻¹ instability, (2) the 120 cm⁻¹ mode similar to the KT40 soft-mode. (3) All other polar eigenvectors and (4) All nonpolar eigenvectors.

ν	(1)	(2)	(3)	(4)	ν	(1)	(2)	(3)	(4)
66	0.3	0.6	0.1	99.0	147	0.1	0.4	17.2	82.4
79	0.1	0.1	0.1	99.7	163	0.1	87.9	8.4	3.6
124	7.2	89.0	1.2	2.7	169	0.8	3.1	84.1	12.0
147	0.0	0.9	0.8	98.2	176	9.9	0.1	85.6	4.3
159	0.0	0.2	21.7	78.1	179	9.4	0.1	84.2	6.3
160	0.6	0.6	77.6	21.3	199	4.4	0.1	94.2	1.2
176	0.1	0.4	23.2	76.3	205	7.0	3.1	59.9	30.0
178	0.0	0.1	80.5	19.4	210	2.8	1.5	14.8	80.8
187	1.3	0.9	91.4	6.4	215	0.2	1.9	35.5	62.5
199	0.5	0.6	91.6	7.3	235	22.4	0.2	60.7	16.6
199	0.5	0.3	51.7	47.5	262	30.8	1.0	57.5	10.6
206	3.3	1.1	46.6	49.1	290	5.0	0.2	2.2	92.7
224	0.2	0.1	10.2	89.5	337	2.2	0.1	96.7	1.1
239	7.3	0.6	70.7	21.4	362	0.0	0.0	96.7	3.3
247	1.6	0.1	6.2	92.2	417	0.0	0.0	24.4	75.6
252	6.1	0.3	20.8	72.8	428	2.8	0.0	0.9	96.3
262	0.0	0.0	0.7	99.3	444	0.4	0.0	63.9	35.7
307	55.1	3.4	17.7	23.9	449	1.4	0.0	0.8	97.7
332	0.8	0.1	0.8	98.3	459	0.1	0.0	13.3	86.6
335	0.8	0.0	14.6	84.6	565	0.1	0.2	99.5	0.2
336	0.2	0.0	63.6	36.3	864	0.0	0.0	99.5	0.4
342	0.0	0.0	25.3	74.7					
351	0.3	0.0	5.6	94.2					
378	13.5	0.6	77.2	8.7					
432	0.0	0.0	99.7	0.3					
528	0.1	0.0	15.1	84.8					
542	0.0	0.0	3.3	96.7					
561	0.1	0.0	81.7	18.3					
622	0.0	0.0	0.7	99.2					
857	0.0	0.0	99.6	0.4					
909	0.1	0.0	0.3	99.6					

TABLE VII: $F_{1u} \rightarrow E + A_1$ splitting of the KLT TO soft mode for various supercells at fixed $a = 3.9879\text{\AA}$. Experimental results are given for $x = 0.05$. Frequencies are in cm⁻¹.

supercell	x	$\nu_{TO} (E)$	$\nu_{TO} (A_1)$	splitting
KT40	0	(76)	(76)	0
KLT80a	0.0625	79	139	60
KLT40	0.125	85	197	112
Experiment ³⁹	0.05	$c. 50$	$c. 80$	$c. 30$

but the A_1 soft-mode component frequency increases by only about 0.04 cm^{-1} , owing to the small participation of Li in this mode. The E -mode frequency increase is an order of magnitude smaller.

Computed, averaged, infrared reflectivity spectra for poled KLT40 and KT at the equilibrium lattice constant are compared in Fig. 4. The two spectra are generally similar, but in KLT40, KT-bands are split by symmetry-breaking Li-displacements.

C. Isolated Li-Ions

Li-ions can jump between nn $[0, 0, d]_c$ wells via $[1, 1, 0]_c$ saddle points. Fig. 5 shows the computed Li potential between nn Li-wells; e.g. $[0, 0, d]_c$ and $[0, d, 0]_c$ via a minimum energy $[0, 1, 1]_c$ saddle. Li-ions were moved along a straight line between the wells. The energetics of Li motion, with all non-Li ions fixed in the positions that they occupy when Li is in its equilibrium off-center state, are contrasted with the energetics for Li motion in conjunction with correlated relaxations of non-Li ions. Note that these frozen coordinates differ from those in Fig. 2 where all non-Li ions occupy positions that are consistent with a center of symmetry. Clearly, ionic relaxation promotes Li-hopping by reducing potential barriers. Fully relaxed calculations yield reasonable agreement with results obtained from Arrhenius fits to NMR data². The fixed-ion potential barrier is $\sim 103 \text{ meV}$ (1190 K). The experimental value, 86 meV (1000 K) [3] is lower, but the value 103 meV (1200 K) [11] is close. A similar potential barrier value was also obtained in the KLT80a computation. Note that computed barrier heights will be systematically larger than values obtained by experiment if the latter are reduced by Li-tunneling.

D. Li-Li Pairs

The energetics of Li-Li nn pair displacement configurations were studied using the KLT80a supercell (Fig. 6) for all nn-pair configurations listed in Table VIII. Total energy calculations, with all ions relaxed and $a = 4 \text{ \AA}$, indicate that the lowest energy path for converting the minimum energy $z - z$ configuration into the $\bar{z} - \bar{z}$ configuration is via intermediate microstates; e.g. the energy for $z - z \rightarrow x - y$ is 2627 K (Table IX) within the experimentally reported range of values, $2100\text{-}2800 \text{ K}$,^{11,12,13} attributed to the rearrangement of Li-Li nn-pairs.¹⁰ Barrier height computations for two selected low-energy paths (see Fig. 7) were performed by converting the $z - z$ configuration into $\bar{z} - \bar{z}$ via intermediate states (Fig. 6). Note that the metastable states are separated by high barriers the lowest of which, 356 meV (4130 K), is significantly larger than the value $2100\text{-}2800 \text{ K}$ ^{11,12,13} obtained by fitting an Arrhenius expression to experimental data; this discrepancy may be explained by Li-tunneling

TABLE VIII: Fully relaxed Li-Li pair configurations in KLT80b (no subscript), KLT80c (subscript 2), KLT80d (3) and KLT80e (4). Li-displacement vectors from ideal perovskite positions are given in \AA .

notation	x_1	y_1	z_1	x_2	y_2	z_2	$E[\text{eV}]$
$z - z$	0.00	0.00	1.43	0.00	0.00	1.19	0.000
$x - z$	1.18	0.00	0.06	-0.01	0.00	1.31	0.124
$x - \bar{z}$	1.11	0.00	-0.02	0.00	0.00	-1.12	0.221
$y - x$	0.00	1.12	-0.01	1.12	0.00	0.01	0.227
$x - x$	1.07	0.00	0.00	1.07	0.00	0.00	0.257
$x - \bar{x}$	1.10	0.00	-0.01	-1.10	0.00	0.01	0.279
$\bar{z} - z$	0.00	0.00	-1.09	0.00	0.00	1.09	0.335
$z - \bar{z}$	0.00	0.00	0.76	0.00	0.00	-0.76	0.550
$x - x_2$	1.14	0.01	-0.01	1.13	0.01	-0.01	0.141
$x - z_2$	1.11	0.00	-0.02	0.03	0.00	1.13	0.213
$x - \bar{y}_2$	1.11	-0.02	0.01	0.02	-1.11	0.01	0.216
$z - \bar{z}_2$	0.00	0.00	1.14	0.00	-0.00	-1.16	0.235
$x - y_2$	1.14	0.03	-0.01	0.04	1.14	-0.02	0.258
$z - z_2$	0.00	-0.03	1.09	0.00	-0.00	1.09	0.275
$x - \bar{x}_2$	1.10	-0.02	-0.00	-1.18	-0.05	0.01	0.383
$z - z_3$	-0.01	0.00	1.14	-0.01	0.00	1.14	0.138
$z - x_3$	0.03	0.01	1.12	1.12	-0.02	0.03	0.229
$\bar{z} - z_3$	0.01	-0.01	-1.09	0.00	0.00	1.09	0.385
$z - x_4$	-0.02	0.00	1.14	1.11	0.00	-0.01	0.213
$z - z_4$	0.00	0.00	1.09	0.00	0.00	1.08	0.248
$z - \bar{z}_4$	0.00	0.00	1.10	0.00	0.00	-1.10	0.257

TABLE IX: Excitation energies for Li-Li nn-pairs (K).

notation	$z - z$	$x - z$	$x - \bar{z}$	$y - x$	$x - x$	$\bar{z} - z$	$x - \bar{x}$	$z - \bar{z}$
$z - z$	0							
$x - z$	1432	0						
$x - \bar{z}$	2570	1138	0					
$y - x$	2627	1195	57	0				
$x - x$	2990	1558	420	363	0			
$x - \bar{x}$	3170	1738	600	543	180	0		
$\bar{z} - z$	3883	2451	1313	1253	893	713	0	
$z - \bar{z}$	6379	4947	3809	3752	3389	3209	2496	0

between metastable states that are close in energy. Ionic potentials were computed, at fixed lattice parameters, in a two-step sequence: 1) A Li-ion in a Li-Li nn pair was moved along a straight line between nn equilibrium states, while other ionic coordinates (including those of the second Li ion) were fully relaxed. 2) The second Li-ion was moved along a straight line between nn wells while all other ionic coordinates (including those of the first Li ion) were fully relaxed. Simultaneous motions of both ions in a Li-Li pair were tried, but this path required greater energy. Hence, Li dynamics within Li-Li pairs is Glauber type.⁴² Significantly, the excitation energy for $z - z \rightarrow x - x$ Li-Li nn-pair flipping is close to the energy for $z - z \rightarrow x - \bar{x}$ and $z - z \rightarrow x - y$ flipping. These

results are inconsistent with the classic dipole-dipole interaction expression $E \propto (\vec{\mu}_1 \cdot \vec{\mu}_2) - 3(\vec{\mu}_1 \cdot \hat{r}_{12})(\vec{\mu}_2 \cdot \hat{r}_{12})$.

If the experimental observation of two relaxation processes^{11,12} corresponds to flipping of isolated Li-ions and Li-Li nn-pairs, then significant concentrations of both must be present. Assuming a random distribution of Li-ions in KLT, one can calculate the densities of isolated Li-ions and Li-Li nn pairs as functions of x ; $x(1-x)^6$, and $3x^2(1-x)^{10}$, respectively (Fig. 8).

The average distance between Li-Li nn-pairs is obviously larger than the average distance between isolated Li-ions because the concentration of Li-Li nn-pairs (x_{Li-Li}) is so much lower ($x_{Li-Li} \approx 3x^2$ for small x). Therefore, it is plausible to think of randomly oriented but interacting PNC that each contain one Li-Li nn-pair as the “seed” plus several isolated Li-ions. Such a system has an interesting phase diagram.¹⁵ Because the energy required to reorient the polarization axis of a Li-Li nn-pair by 90° is large, 2990 K, PNC polar orientations resist coarsening that involves reorientation(s) of Li-Li nn-pair axes. This constraint on FE-percolation⁷ may explain the observation of a dipole-glass like state in KLT^{3,5} with $0 < x < 0.02$.

Results for supercells with two Li-ions, separated by more than a_0 , are given in Table VIII. For example, KLT80e has three symmetry-independent configurations (Fig. 9): (1) both Li-ions are displaced in the same direction, $z - z_4$; (2) they are displaced in opposite directions; $z - \bar{z}_4$; (3) they are displaced in perpendicular directions, e.g. $z - x_4$. The $z - x_4$ configuration has lowest energy at fixed lattice parameter. This may be a consequence of accommodating two off-centered Li-ions, each of which produces a strong local tetragonal distortion, into a cell in which the global strain is constrained to be zero.

Stachiotti *et al.*⁴³ used a shell model to compute Li-Li interactions in KLT out to distance $6 a_0$. Their results also indicate large strain-, and nonlinear polarization corrections, to the dipole-dipole interaction energy. Experimental diffuse scattering data for KLT⁴⁴ indicate strongly correlated planar atomic displacements rather than chain-displacements as observed in KNbO₃, BaTiO₃, KTaO₃ and SrTiO₃.^{45,46,47,48}

E. Dynamical Charges and Polarization

The polarization induced by Li off-centering was studied by Berry phase analyses, and dynamical charges $Z_{\alpha\alpha}^*$ were determined for all ions in KLT40_{Ref}, fully relaxed KLT40 (Table X), and KLT40 with ions in ideal perovskite positions (Table XI). Compare these charges with Z_{zz} in KT with the same lattice parameter: K: 1.151; Ta: 8.680; O_x: -1.690; O_y: -1.690; O_z: -6.452.

The dynamical charge is a symmetric function of displacements (u) from ideal perovskite positions, so to a first approximation, it is quadratic in u :

$$Z_{zz}^*(u) = Z_{zz}^*(0) - \zeta u^2 \quad (1)$$

TABLE X: Dynamical charges Z_{zz}^* in the KLT40 supercell.

Ions		x	y	z	Z_{zz}^*	Z_{xx}^*	Z_{yy}^*
K ₁	1a	0.0000	0.0000	0.0014	1.445	1.142	1.142
K ₂	2c	0.5000	0.0000	0.9996	1.024	1.180	1.132
K ₃	2c	0.5000	0.0000	0.4963	1.014	1.168	1.122
K ₄	1a	0.0000	0.0000	0.4952	0.999	1.146	1.146
K ₅	1b	0.5000	0.5000	0.0074	1.402	1.177	1.177
Li	1b	0.5000	0.5000	0.6273	0.574	1.106	1.106
Ta ₁	4d	0.2513	0.2513	0.2526	8.145	8.745	8.745
Ta ₂	4d	0.2494	0.2494	0.7499	8.619	8.479	8.479
O ₁	4d	0.2515	0.2515	0.9935	-6.003	-1.685	-1.685
O ₂	4d	0.2474	0.2474	0.4957	-6.232	-1.639	-1.639
O ₃	4e	0.0000	0.2500	0.2436	-1.724	-6.382	-1.738
O ₄	4e	0.0000	0.2533	0.7457	-1.661	-6.358	-1.619
O ₅	4f	0.5000	0.2482	0.2442	-1.651	-6.662	-1.644
O ₆	4f	0.5000	0.2589	0.7379	-1.617	-6.197	-1.790

TABLE XI: Dynamical charges Z_{zz}^* , ionic displacements (in Å) and total dipole moment (in eÅ) in the KLT40 supercell. Only symmetrically distinct ions are listed: for ionic coordinates see Table V.

Ions	Refer. struct.	Ideal perov. positions	Average dyn. ch.	Displ. [Å]	Tot. dip. [eÅ]
K ₁	1.153	1.152	1.250	0.011	0.014
K ₂	1.153	1.151	1.109	-0.003	-0.007
K ₃	1.153	1.153	1.107	-0.029	-0.064
K ₄	1.153	1.153	1.102	-0.038	-0.042
K ₅	1.153	1.124	1.217	0.058	0.071
all K			1.143	-0.005	-0.029
Li	1.251	1.251	1.025	1.009	1.035
Ta ₁	8.713	8.710	8.522	0.021	0.706
Ta ₂	8.714	8.712	8.681	-0.001	-0.035
all Ta			8.602	0.010	0.670
O ₁	-6.450	-6.472	-6.315	-0.051	1.293
O ₂	-6.529	-6.504	-6.413	-0.034	0.867
all O			-6.364	-0.042	2.160
O ₃	-1.703	-1.700	-1.708	-0.051	0.346
O ₄	-1.700	-1.700	-1.687	-0.034	0.231
O ₅	-1.687	-1.685	-1.673	-0.046	0.306
O ₆	-1.687	-1.685	-1.662	-0.096	0.637
all O _⊥			-1.683	-0.057	1.521
all O					3.681
Total					5.357
Exact value					5.153

The average dynamical charge, which is required for calculating the polarization, is

$$\langle Z_{zz}^* \rangle = \frac{1}{u_1 - u_0} \int_{u_0}^{u_1} Z_{zz}^*(u) du =$$

$$= Z_{zz}^*(0) + \frac{1}{3}\zeta (u_1^2 + u_0^2 + u_1u_0) \quad (2)$$

In particular, if $u_0 = 0$ then

$$\langle Z_{zz}^* \rangle = \frac{1}{3} (Z_{zz}^*(u_1) + 2Z_{zz}^*(0)) \quad (3)$$

Average values of the dynamical charges, and individual ion contributions to the total KLT40 supercell dipole moment are listed in Table XI. For comparison, the explicit value of the total dipole moment, obtained by Berry phase analysis, is also shown.

The largest contribution to the total dipole moment is from O ions. The Li-displacement contribution is roughly equal to that of Ta. The total dipole moment is ~ 5 times larger than the dipole moment due to the Li ion itself, which indicates that the Li-dipole moment is strongly *enhanced* by structural relaxation.

A similar enhancement was also obtained in a shell model calculation,⁴⁹ but in that study the main cause of enhancement was a large Ta-displacement. Here, enhancement of the Li-dipole moment is primarily caused by coupling between Li- and O-displacements.

TABLE XII: The KLT80b supercell dipole moment (in $e\text{\AA}$) for different Li-Li nn-pair configurations

notation	direct.	K	Li	Ta	O $_{\perp}$	O $_{\parallel}$	Total
$z-z$	z	0.138	2.688	4.636	2.215	3.850	13.527
$x-\bar{z}$	z	-0.170	-1.168	-3.702	-1.432	-2.524	-8.996
	x	0.335	1.138	4.915	1.085	1.888	9.361
$x-x$	x	0.393	2.184	5.681	2.079	3.417	13.754
$x-z$	z	0.152	1.408	3.830	1.187	2.202	8.779
	x	0.512	1.193	6.315	0.580	1.008	9.608
$y-x$	y	0.393	1.147	5.451	0.867	1.480	9.338
	x	0.393	1.147	5.451	0.867	1.480	9.338

Total dipole moments for a KLT80b supercell with different Li-Li nn-pair configurations are listed in Table XII. They were calculated with the average dynamical charges listed in Table XI and ionic displacements relative to ideal perovskite. Individual ionic contributions are also shown. Oxygen ion contributions are separated into O $_{\parallel}$ and O $_{\perp}$, with the polarization direction parallel and perpendicular to the Ta-O-Ta bond, respectively. These results indicate that the total dipole moment induced by Li-Li pairs is larger than that from two isolated Li-ions.

F. Coupling Between Strain and Polarization

The influence of applied stress on dipole moment and energy was studied by applying various tetragonal distortions to the KLT40 supercell with $a = 3.95594 \text{ \AA}$, and $0.98a < c < 1.02a$. Total energy calculations show that, for $c > a$, configurations with $[0, 0, 1]_c$ -displaced Li-ions

are lower in energy than those with $[1, 0, 0]_c$ -displaced Li. The difference in energies is

$$-\delta E_{zz}[\text{meV}] = 1.649e_3 + 105.7e_3^2 + 3430.e_3^3 \quad (4)$$

where $e_3 = (c/a - 1)$. By using this energy difference, the occupation probability for Li-displacements in the c -direction can be estimated as

$$w_{-z-z} = w_{zz} = \frac{e^{-\delta E_{zz}/k_B T}}{4 + 2e^{-\delta E_{zz}/k_B T}} \approx 1/6 - \delta E_{zz}/9k_B T \quad (5)$$

Hence, tetragonal strain increases the population of Li-displacements parallel to the c -axis. The energy decrease (per primitive cell) connected with redirected Li-ions is,

$$\langle \delta E_{Lizzzz} \rangle = x\delta E_{zz}(w_{-z-z} + w_{zz} - 1/3) \approx -2x\delta E_{zz}^2/9k_B T \quad (6)$$

which at small e_3 , is proportional to e_3^2 . Thus, the energy decreases by local Li-redirections along c and this decreases the corresponding elastic constant proportionally to x .

Li-redirectation also increases the square of supercell dipole moment d_z along the c -axis

$$\delta q_{zzzz} = d_z d_z (w_{zz} + w_{-z-z} - 1/3) \approx 2d_z^2 \delta E_{zz}/9k_B T. \quad (7)$$

By comparison with (4), δq_{zzzz} is proportional to strain for small e_3 . Because Li-redirectation is coupled to strain, one expects a relaxation contribution to the electrostriction constants and acoustic response, as observed by Pattnaik and Toulouse [^{11,50}].

In addition to promoting Li-redirectation, tetragonal distortions change the TO soft mode frequency. Using the average dynamical charges and computed ionic displacements, one can calculate supercell dipole moments, d_z and d_x in $e\text{\AA}$, which correspond to Li-ions displaced in the $[0, 0, 1]_c$ and $[1, 0, 0]_c$ directions respectively, for $a < c < 1.2a$:

$$d_z = 5.15 + 167.e_3 + 2987.e_3^2 \\ d_x = 5.15 - 40.e_3 + 585.e_3^2 \quad (8)$$

These results show that the supercell dipole moment is greatly enhanced by an increase in c/a . Partial contributions to the dipole moment that are associated with Ta- and O-displacements are most sensitive to changes in c ; which is consistent with an electrostriction induced reduction in the soft-mode frequency.

G. Toward an Effective Hamiltonian

The picture of KLT in which Li-dipoles, a soft-mode, and PNC all interact, lends itself to a first-principles based effective Hamiltonian, H_{eff} , treatment. Full formulation of H_{eff} is beyond the scope of this work, but some essential intermediate results have been derived. For simplicity, consider KLT40, with the same ionic displacements in each unit cell.

To derive H_{eff} for a FE, one selects a local basis for the instabilities that cause the FE transition, and includes interactions between sites, between local distortion and strain, etc.⁵¹. In KLT, it is clear that instabilities centered on Li are responsible for the phase transition, and that Li-centered distortion variables must be included in H_{eff} . However, the coupling of Li-dipole moments to the KT soft-mode is sufficiently important that one must also include a local variable for the KT soft-mode. By analogy with H_{eff} for KNbO_3 ⁵², this local variable is centered on the Ta sites.

Several eigenvectors are relevant:

- $v_{1,\alpha}$: the dynamical matrix eigenvector for the KT soft-mode, polarized along $\hat{\alpha}$.
- $v_{2,\alpha}$: the dynamical matrix eigenvector for the Li-instability of KLT40, polarized along $\hat{\alpha}$. (Dynamical matrix eigenvectors are normalized for 40-atom cells).
- $v_{Ta,\alpha} = v_{1,\alpha}$ and $v_{Li,\alpha} = v_{2,\alpha}$, orthogonalized to $v_{1,\alpha}$, and renormalized.
- $d_{Li,\alpha}$ and $d_{Ta,\alpha}$, the dimensionless displacement eigenvectors obtained by dividing the elements of $v_{Ta,\alpha}$ and $v_{Li,\alpha}$, respectively, by $\sqrt{(m/m_0)}$, where (arbitrarily) mass $m_0 = 1$ amu.

Consider displacement patterns in KLT40 in which displacement amplitudes corresponding to $v_{Ta,\alpha}$ and $v_{Li,\alpha}$ are τ_α and λ_α , respectively. The energy is minimized with respect to all other modes. The strain tensor is $\{e_i\}$, $i = 1, 6$, in Voigt notation. Calculated results closely fit the expansion:

$$\begin{aligned}
U &= U_o \\
&- 0.055566|\lambda|^2 + 0.004160|\lambda|^4 \\
&+ 0.016303(\lambda_x^2\lambda_y^2 + \lambda_x^2\lambda_z^2 + \lambda_y^2\lambda_z^2) \\
&- 0.000077|\lambda|^6 + 0.000001|\lambda|^8 \\
&+ 0.024760|\tau|^2 + 0.008677|\tau|^4 \\
&- 0.011288(\tau_x^2\tau_y^2 + \tau_x^2\tau_z^2 + \tau_y^2\tau_z^2) + 0.000684|\tau|^6 \\
&- 0.025236\vec{\lambda} \cdot \vec{\tau} + 0.001210(\lambda_x^3\tau_x + \lambda_y^3\tau_y + \lambda_z^3\tau_z) \\
&- 0.000370(\lambda_x\tau_x(\lambda_y^2 + \lambda_z^2) + \text{cyclic perm.}) \\
&+ 817.342(e_1^2 + e_2^2 + e_3^2) + \\
&+ 210.580(e_1e_2 + e_1e_3 + e_2e_3)
\end{aligned}$$

$$\begin{aligned}
&+ 732.803(e_4^2 + e_5^2 + e_6^2) \\
&- 0.262724(e_1\lambda_x^2 + e_2\lambda_y^2 + e_3\lambda_z^2) \\
&- 0.209816(e_1(\lambda_y^2 + \lambda_z^2) + e_2(\lambda_x^2 + \lambda_z^2) + \\
&+ e_3(\lambda_x^2 + \lambda_y^2)) \\
&- 5.30307(e_4\lambda_y\lambda_z + e_5\lambda_x\lambda_z + e_6\lambda_x\lambda_y) \\
&- 3.24098(e_1\tau_x^2 + e_2\tau_y^2 + e_3\tau_z^2) \\
&+ 0.715628(e_1(\tau_y^2 + \tau_z^2) + e_2(\tau_x^2 + \tau_z^2) + \\
&+ e_3(\tau_x^2 + \tau_y^2)) \\
&+ 1.38297(e_4\tau_y\tau_z + e_5\tau_x\tau_z + e_6\tau_x\tau_y),
\end{aligned} \tag{9}$$

where U is in eV and $\vec{\lambda}$ and $\vec{\tau}$ in Å. The connection between TO polarization and τ is, $P_{TOz} = 3.766820\tau_z/V$ eÅ where V is the unit cell volume. The connection between the Li-dipole moment and $\vec{\lambda}$ is, $\mu_z = 0.876855\lambda_z$ eÅ.

The potential for $\vec{\lambda}$ alone (\sim Li off-centering) has 6 wells in $[0, 0, 1]_c$ directions. The potential for $\vec{\tau}$ alone (KT soft-mode) has a small positive harmonic coefficient and is therefore highly polarizable. Negative bilinear coupling between $\vec{\lambda}$ and $\vec{\tau}$ indicates that the soft-mode enhances the total polarization from Li off-centering. Positive coefficients of $|\tau|^4$ and $|\tau|^6$ imply that the soft-mode frequency hardens as the structure distorts. Higher-order coupling between $\vec{\lambda}$ and $\vec{\tau}$ is included because it significantly improves the fit.

One can reduce the number of variables by excluding strain. This results in a decrease of the nonlinearity constant which multiplies the fourth power of polarization, and changes the sign of the angle dependent term for the soft-mode.

Eq. 9 and the mode effective charges can be used to calculate the soft-mode and Li-dipole contributions to the susceptibility. The soft-mode contribution is 110 for the reference state, much less than might be expected considering that KT is an incipient ferroelectric. The LDA overestimates the soft mode frequency of KT, which leads to too large a value for the $|\tau|^2$ coefficient of Eq. 9 and too low a permittivity. For fully relaxed KLT40, the model predicts that the contribution of the soft-mode to the susceptibility along the polar axis is about 55 due to mode hardening. The Li-dipole contribution is insignificant (order 1). This, however, is only the contribution to the static susceptibility from Li vibrating within a single well. As discussed in Section IV, Li-hopping gives a much greater, frequency-dependent, contribution to the susceptibility.

From Eq. 9 and the mode effective charges, the coupling between TO phonons and Li-dipoles is $0.064\mu_z P_{TOz}/3V\varepsilon_0$ where ε_0 is the permittivity of free space. This coupling enhances dielectric permittivity and shifts the Curie temperature to higher values (c.f. Sec IV). This Lorentz factor, 0.064, is smaller than that found⁴ in a point polarizable ion model, (0.1 - 0.2). The Lorenz factor decreases quadratically with Li displace-

ment and equals 0.037 at the equilibrium Li position.

To complete H_{eff} requires: (1) Formulating local representations of $\vec{\lambda}$ and $\vec{\tau}$ e.g. lattice Wannier functions⁵³); (2) Quantifying distance dependencies of the interactions^{51,54}.

H. Band Structure Calculations

Strong n-type photocurrent is observed in KLT at $T \lesssim 80K$ ²², and it has been attributed to shallow $O_6 2p$ hole states at the bottom of the valence band which are caused by large O_6 -displacements (notation of Table V). Holes are trapped by these levels which prevent recombination with electrons that were promoted to the conduction band by light absorption.

To study shallow forbidden gap states in KLT, band-structure calculations were performed for KLT40 and the corresponding ideal $KTaO_3$ supercell, in the $\Gamma - X$ direction. Results for the top of valence and bottom of conduction bands are shown in Fig. 10. The top of the valence band, and the bottom of the conduction band, are split and/or distorted in KLT40 relative to KT.

VASP results confirm large O_6 -displacements,²² and demonstrate some splitting at the top of the valence band, and some distortion at the bottom of the conduction band. This occurs because Li off-centering breaks $Pm\bar{3}m$ symmetry creating symmetrically different O-ions with different self-consistent electrostatic potentials (cf. Ref.⁵⁵). The VASP results, however, do not confirm the presence of $O_6 2p$ states at the top of the valence band.

TABLE XIII: Electrostatic potentials (in eV) on the ions of the KLT40 supercell in the equilibrium structure (Equil), reference structure (Refer), and in pure KT (KT). Only symmetrically distinct ions are listed (atomic positions are listed in Table V).

Ion	Equil.	Refer.	KT	Ion	Equil.	Refer.	KT
K_1	10.15	10.18	10.33	K_2	10.13	10.15	10.33
K_3	10.18	10.23	10.33	K_4	10.15	10.15	10.33
K_5	10.14	10.23	10.33	Li	43.90	42.68	
Ta_1	-1.21	-1.22	-1.30	Ta_2	-1.29	-1.22	-1.30
O_1	-56.27	-56.26	-56.07	O_2	-56.30	-56.30	-56.07
O_3	-56.19	-56.26	-56.07	O_4	-56.46	-56.26	-56.07
O_5	-56.28	-56.31	-56.07	O_6	-56.43	-56.31	-56.07

Computing the electrostatic potentials on different ions in KLT40 (Table XIII) reveals that the $O_6 2p$ states are significantly deeper in fully relaxed KLT40 than in KT or $KLT40_{Ref}$. The same result was obtained from projections of band states onto $O_6 2p$ states: $O_6 2p$ -states in KLT40 lie below the top of the valence band. Similar results were obtained for Li-Li nn pairs in KLT80, where the tetragonal distortion from Li also causes valence and conduction band splitting.

IV. PHENOMENOLOGY

A. Li-pair relaxation time

Consider KLT as a distribution of PNC (containing one or more Li-ions) in a KT lattice. FP calculations on isolated Li-ions and on Li-Li pairs have shown that each PNC may have a set of states defined by the Li-displacement directions. For a given PNC, group theory can be used to enumerate distinct relaxation processes and identify which of them couple to an electric field. The kinetic equations for state occupation probabilities can be solved to estimate the relaxation times. If PNC do not interact, then there are distinct relaxation times for each cluster type, and the relaxational contribution to the dielectric function is the sum of contributions from each cluster. Interactions between clusters will broaden an otherwise sharp distribution of relaxation times.

For isolated Li-ions, there are six states, and symmetry analysis of relaxation processes yields $A_{1g} + E_g + F_{1u}$. The A_{1g} “process” is the trivial steady state equilibrium solution. Only the F_{1u} process couples with an electric field and affects dielectric dispersion. The E_g process couples with stress, but not electric field. Let k be the hopping rate between wells separated by 90° and neglect hopping between wells separated by 180° . Then relaxation time $\tau^{-1} = 4k$ for the F_{1u} and $\tau^{-1} = 6k$ for the E_g process².

For Li-Li nn-pairs, there are 36 states, many of which are metastable (Table IX). Symmetry analysis identifies seven relaxation processes that contribute to the dielectric function. Six of these involve substantial probability redistribution among metastable states whose occupancies are negligible. Thus, only one relaxation process contributes significantly to the dielectric function; the one whose net effect is $z - z \rightleftharpoons \bar{z} - \bar{z}$.

The full set of kinetic equations give a 36×36 matrix. For simplicity, consider only the states that are associated with the minimum energy path in Fig. 7:

$$\begin{aligned}
-\frac{dw_a}{dt} &= k_{ab}w_a - k_{ba}w_b \\
-\frac{dw_b}{dt} &= (k_{ba} + k_{bc})w_b - k_{ab}w_a - k_{cb}w_c \\
-\frac{dw_c}{dt} &= 2k_{cb}w_c - k_{bc}w_b - k_{bc}w_d \\
-\frac{dw_d}{dt} &= (k_{bc} + k_{ba})w_d - k_{cb}w_c - k_{ab}w_e \\
-\frac{dw_e}{dt} &= k_{ab}w_e - k_{ba}w_d
\end{aligned} \tag{10}$$

where w_α is occupation probability for well α . The relaxation time of the dominant process is:

$$\tau^{-1} = (k_{ab} + k_{ba} + k_{bc})/2 - \sqrt{a^2 - k_{ab}k_{ba}}, \tag{11}$$

Here $a = (k_{ab} + k_{ba} + k_{bc})/2$.

In the realistic limit $k_{ab} \sim k_{bc} \ll k_{cb} \sim k_{ba}$: $\tau^{-1} \simeq k_{bc}k_{ab}/k_{ba}$. This rate corresponds to overcoming the principle Li-Li nn-pair barrier ($z - z \rightarrow x - x$) in the $z - z \rightleftharpoons \bar{z} - \bar{z}$ process.

B. Dielectric-permittivity frequency-dependence

If one excludes strains from a mean field Hamiltonian then there are two variables: one for a soft-mode; the other for Li-dipoles. Both contribute to the dielectric response, but the former is essentially dispersionless far below the soft-mode frequency. The Li-dipole term however has relaxational character. Neglecting the damping of Li-oscillations in Li wells, but accounting for jumps between nn Li-wells, the Li-dipole associated with z -polarization of an isolated Li-ion in a cubic environment is:

$$D_z = \frac{x\mu_z}{V}(w_z - w_{-z}) \quad (12)$$

where V is the primitive unit cell volume. The F_{1u} relaxation process contributes to polarization fluctuations, and the polarization takes the form⁵⁶

$$D_z = \varepsilon_0 F(T) \tilde{E}_z \quad (13)$$

where

$$F(T) = \frac{x\mu_z^2}{V\varepsilon_0} \frac{1}{6k_B T} \frac{1}{4k + i\omega} \quad (14)$$

Here: $\tilde{E}_z = E_z + \lambda P_{TOz}$ is the local field, $\lambda = \lambda_0 - 3\lambda_1\mu^2$ a coupling constant, λ_0 and λ_1 are the effective Hamiltonian coefficients of $-\mu_z P_{TOz}$ and $\mu_z^3 P_{TOz}$ respectively; E_z is an external field; P_{TOz} is the polarization connected with the soft-mode; and $\tau = 4k$ is the relaxation time for the F_{1u} relaxation process. The dielectric susceptibility connected with Li jumps can be now written as^{4,56,57}

$$\chi_{Li} = \frac{F(T)}{1 - \lambda^2 F(T) \varepsilon_0 / A(T)} \quad (15)$$

where

$$A(T) = \alpha + 3\beta P_{TOz}^2 + 5\gamma P_{TOz}^4 \quad (16)$$

Here the nonlinearity coefficient β is renormalized after the elimination of strains; α is renormalized due to fields produced by Li. The positive correlation between α and increased x implies hardening of the soft mode with increasing Li concentration. Dielectric susceptibility is enhanced at low frequencies by coupling between

Li-dipoles and the TO soft mode; T_c increases and frequency dispersion is enhanced. These results were obtained by considering all hopping paths between the six $[0, 0, d]_c$ -type wells, not by invoking an Ising model.

The dominant relaxation process for Li-Li nn pairs leads to an additional relaxational contribution to $F(T)$, proportional to Li-Li nn-pair concentration, and with $\tau^{-1} = k_{bc}k_{ab}/k_{ba}$ (cf. results in Refs.^{12,58}). The concentration of Li-Li nn pairs is low, but their dipole moments are large (Table XII), and χ_{Li} is proportional to the dipole moment squared (14).

The temperature dependence of the kinetic coefficient k is common, and it is mainly controlled by the barrier height U . The temperature dependence of the relaxation time is

$$\begin{aligned} \tau &= A\chi(T) \int_{-\infty}^{\infty} e^{(U+ay^2)/k_B T} dy = \\ &= A\chi(T) \sqrt{\frac{\pi k_B T}{a}} e^{U(T)/k_B T} = \\ &= \tau_0(T) e^{U(T)/k_B T}, \end{aligned} \quad (17)$$

where χ is the dielectric permittivity of the media in which the PNC are embedded and a is a constant determined by the force constants at the saddle point.

V. CONCLUSIONS

Calculations on a 40-atom KLT40 supercell that contains one Li-ion indicate that there is only one instability connected with Li off-centering. This instability is associated with large Li-displacement in the $[0, 0, 1]_c$ direction. Li potential wells are separated by potential barriers with $[1, 1, 0]_c$ saddles. Calculated $[1, 1, 0]_c$ potential barriers and $[0, 0, d]_c$ Li-displacements, in fully relaxed KLT, are in good agreement with values obtained by fitting a mean field expansion to experimental data^{11,12}.

All ions in the KLT40 supercell are displaced from ideal perovskite positions, but the O-ions closest to Li exhibit the largest sympathetic displacements, towards Li. Calculated vibrational frequencies for fully relaxed KLT40 indicate that A_1 - and E -symmetry modes emanate from an F_{1u} TO mode similar to the soft mode of pure KT. The average frequency of these modes is higher than that of the TO soft mode, which reflects hardening of the soft-mode induced by substituting Li for K. The intrawell Li vibrational frequency is about 300 cm^{-1} . The soft-mode and Li-polarization are coupled.

Berry phase analyses yielded total dipole moments associated with Li off-centering that are ~ 5 times larger than the Li-dipole moment itself. This enhancement is primarily caused by O-relaxation around the off-centered Li-ion.

Fully relaxed KLT40 is tetragonal with $c/a > 1$, and polarization along the c -axis. Polarization increases with

increasing c/a ; uniaxial strain.

First-principle calculations of Li-Li nn-pair excitations in a KLT80 supercell strongly support the conclusion of Dousenau et al.¹⁰ that the “180°” relaxation process is caused by $z - z \rightleftharpoons \bar{z} - \bar{z}$ Li-Li nn-pair flipping.

Acknowledgment

We thank G. Kresse for providing an LDA pseudopotential for Ta. S.A.P. appreciates support from RFBR

grant # 01-02-16029 and thanks NIST for hospitality.

-
- ¹ G.A. Samara, B. Morosin. *Phys. Rev. B* **8**, 1256 (1973).
² J. J. van der Klink and F. Borsa, *Phys. Rev. B* **30**, 52 (1984).
³ U. T. Höchli, K. Knorr and A. Loidl, *Adv. Phys.* **39**, 405 (1990).
⁴ B. E. Vugmeister and M. D. Glinchuk, *Rev. Mod. Phys.* **62**, 993 (1990).
⁵ W. Kleemann, V. Schönknecht, D. Sommer, and D. Rytz, *Phys. Rev. Lett.* **66**, 762 (1991).
⁶ P. Voigt and S. Kapphan, *J. Phys. Chem. Sol.* **55**, 853 (1994).
⁷ S. A. Prosandeev, V. S. Vikhnin, S. Kapphan, *Eur. Phys. J. B* **15**, 469 (2000).
⁸ H. M. Christen, U. T. Höchli, A. Chatelain, and S. Ziolkiewicz, *J. Phys.: Condens. Matter* **3**, 8387 (1991).
⁹ P. Doussineau, T. de Lacerda-Arôso and A. Levelut, *J. Phys.: Condens. Matter* **12**, 1461 (2000).
¹⁰ P. Doussineau, Y. Farssi, C. Frenos, A. Levelut, K. McEneaney, J. Toulouse, S. Ziolkiewicz, *Europhys. Lett.* **24**, 415 (1993).
¹¹ R. K. Pattnaik, J. Toulouse, and B. George, *Phys. Rev. B* **62**, 12820 (2000).
¹² S. A. Prosandeev, V. A. Trepakov, M. E. Savinov, L. Jastrabik, and S. E. Kapphan, *J. Phys.: Condens. Matter* **13**, 9749 (2001).
¹³ U. T. Höchli, J. Hessinger, and K. Knorr, *J. Phys.: Condens. Matter* **3**, 8377 (1991).
¹⁴ P. M. Gehring, S. Wakimoto, Z.-G. Ye, and G. Shirane, *Phys. Rev. Lett.*, **87**, 277601-1 (2001).
¹⁵ A. E. Maslennikov, S. A. Prosandeev, V. S. Vikhnin, S. Kapphan, *Integr. Ferroelectrics* **38**, 797 (2001).
¹⁶ H. Vollmayr, R. Kree, and A. Zippelius, *Phys. Rev. B* **44**, 12238 (1991).
¹⁷ M. P. Ivliev and V. P. Sakhnenko, *Fiz. Tverd. Tela* **28**, 632 (1986).
¹⁸ M. Exner, C. R. A. Catlow, H. Donnerberg and O. F. Schirmer, *J. Phys.: Condens. Matter* **6**, 3379 (1994).
¹⁹ R. I. Eglitis, A. V. Postnikov and G. Borstel, *Phys. Rev. B* **55**, 12976 (1997).
²⁰ I. I. Tupitsyn, A. Deineka, V. A. Trepakov, L. Jastrabik and S. E. Kapphan, *Phys. Rev. B* **64**, 195111 (2001).
²¹ A. V. Postnikov, T. Neumann and G. Borstel, *Ferroelectrics* **164**, 101 (1995).
²² R. S. Klein, G. E. Kugel, M. D. Glinchuk, R. O. Kuzian, I. V. Kondakova, *Phys. Rev. B* **50**, 9721 (1994); V. V. Laguta, M. D. Glinchuk, I. P. Bykov, J. Rosa, L. Jastrabik, R. S. Klein and G. E. Kugel, *Phys. Rev. B* **52**, 7102 (1995).
²³ P. Sangalli, E. Giolotto, L. Rollandi, P. Calvi, P. Camagni, and G. Samoggia, *Phys. Rev. B* **57**, 6231 (1998).
²⁴ P. Galinetti, E. Giolotto, P. Sangalli, P. Camagni and G. Samoggia, *J. Phys.: Condens. Matter* **11**, 9045 (1999).
²⁵ G. Kresse and J. Hafner, *Phys. Rev. B* **47**, 558 (1993).
²⁶ G. Kresse and J. Furthmüller, *Phys. Rev. B* **54**, 11169 (1996).
²⁷ D. Vanderbilt, *Phys. Rev. B* **41**, 7892 (1990).
²⁸ D. J. Singh, *Phys. Rev. B* **53**, 176 (1996).
²⁹ P. Voudsen, *Acta Cryst.* **4**, 373 (1951).
³⁰ G. Shirane, R. Nathans, V. Minkiewisz, *Phys. Rev.* **157**, 396 (1967).
³¹ E. A. Zhurova, V. E. Zavodnik, S. A. Ivanov, P. P. Syrnikov, V. G. Tsirelson, *Z. Naturforsch.* **48a**, 25 (1993).
³² A. V. Postnikov, T. Neumann, G. Borstel, M. Methfessel, *Phys. Rev. B* **48**, 5910 (1993).
³³ Because of weak coupling with another mode with similar frequency, the 205 cm^{-1} mode of pure KT actually is split into 200 cm^{-1} and 205 cm^{-1} modes of KLT40.
³⁴ All results in this paper are calculated using periodic boundary conditions. The results for Li-displacements, etc., include interactions with a periodic set(s) of image Li-ions and do not correspond to the limit of a single Li-ion (single Li-Li pair) in an infinite KTaO_3 lattice.
³⁵ I. Inbar and R. E. Cohen, *Phys. Rev. B* **53**, 1193 (1996).
³⁶ V. Caciuc, A. V. Postnikov, *Phys. Rev. B* **64**, 224303 (2001).
³⁷ H. Vogt, *J. Phys.: Condens. Matter* **7**, 5913 (1995).
³⁸ R. L. Prater, L. L. Chase, and L. A. Boatner, *Phys. Rev. B* **23**, 5904 (1981).
³⁹ R. S. Klein, G. E. Kugel and B. Hennion *J. Phys.: Condens. Matter* **8**, 1109 (1996).
⁴⁰ S. A. Prosandeev, V. S. Vikhnin, and S. Kapphan, *Phys. Stat. Sol. (a)* **172**, 499 (1999).
⁴¹ J. J. vanderKlink and S. N. Khanna, *Phys. Rev. B* **29**, 2415 (1984).
⁴² J. Toulouse, B. E. Vugmeister and R. Pattnaik, *Phys. Rev. Lett.* **73**, 3467 (1994).
⁴³ M. Stachiotti, R. Migoni, J. Kohanoff and U. T. Höchli, *Ferroelectrics* **157**, 335 (1994).
⁴⁴ G. Yong, J. Toulouse, R. Erwin, S. M. Shapiro and B. Hennion, *Phys. Rev. B* **62**, 14736 (2000).
⁴⁵ R. Comes, M. Lambert and A. Guinier, *Acta Cryst. A* **26**, 244 (1970).
⁴⁶ G. Honjo, S. Koderu, and N. Kitamura, *J. Phys. Sac. Jpn* **19**, 351 (1964).
⁴⁷ R. Comes and G. Shirane, *Phys. Rev. B* **5**, 1886 (1972).

- ⁴⁸ R. Wang, Y. Zhu, S. M. Shapiro, Phys. Rev. B **61**, 8814 (2000).
- ⁴⁹ M. G. Stachiotti and R. L. Migoni, J. Phys.: Condens. Matter **2**, 4341 (1990); M.G. Stachiotti, R. L. Migoni, and U. T. Höchli, J. Phys.: Condens. Matter **3**, 3689 (1991).
- ⁵⁰ R. K. Pattnaik and J. Toulouse, Phys. Rev. B **60**, 7091 (1999).
- ⁵¹ W. Zhong, D. Vanderbilt, and K.M. Rabe, Phys. Rev. B **52**, 6301 (1995).
- ⁵² U. V. Waghmare, K. M. Rabe, H. Krakauer, R. Yu, and C.-Z. Wang, in First Principle Calculations for Ferroelectrics, AIP Conference Proceedings 436, edited by R.E. Cohen, AIP, Woodbury, NY (1998), p. 32.
- ⁵³ K. M. Rabe and U. V. Waghmare, Phys. Rev. B **52**, 13236 (1995).
- ⁵⁴ U. V. Waghmare and K. M. Rabe, Phys. Rev. B **55**, 6161 (1997).
- ⁵⁵ S. A. Prosandeev, V. S. Vikhnin and S. E. Kapphan, J. Phys.: Condens. Matter **14**, 4407 (2002).
- ⁵⁶ S. A. Prosandeev, Phys. Sol. St. **43**, 1948 (2001).
- ⁵⁷ C. -C. Su, B. Vugmeister, and A. G. Khachatryan, J. Appl. Phys. **90**, 6345 (2001).
- ⁵⁸ S. A. Prosandeev and V. A. Trepakov, J. Exp. Theor. Phys. **94** 419 (2002).

Captions

Fig. 1. KLT configurations compared on a common 320-atom supercell. The grid connects perovskite A-sites. Empty sites represent K; black circles represent Li. When there is one Li per primitive cell, it is arbitrarily displaced in the \hat{z} direction; when there are two Li per primitive cell, one is displaced in the \hat{z} direction and the other in the \hat{x} direction.

Fig. 2. Structural distortions around Li in KLT40.

Fig. 3. Energy as a function of Li-displacement from an ideal A-site position in KLT40: with all ions' coordinates frozen in the centrosymmetric positions except for Li (a); with full relaxation of all ions' coordinates except for Li (b).

Fig. 4. Comparison of the reflectivity spectra computed for KT and KLT40 (the component along the polar axis (R_z), perpendicular to it (R_x), and averaged spectrum (R_{av})) at identical lattice parameters $a_0 = 3.956 \text{ \AA}$. The electronic permittivity ϵ_∞ was set to 5.15 in each case, the experimental value for KT.⁴¹ The damping constant was set to 20 cm^{-1} for all modes in KT and 40 cm^{-1} for KLT40.

Fig. 5. Li potential barriers in KLT40 in the direction between nearest neighbor Li-wells computed with all ions except Li fully relaxed (relaxed), and with all ions except Li frozen at their coordinates corresponding to Li at its equilibrium position (frozen).

Fig. 6. A-site configurations in KLT80b. Undecorated sites are occupied by K.

Fig. 7. The energetics of Li-Li nearest neighbor pair reorientation, $z - z \rightarrow \bar{z} - \bar{z}$, including the intermediate states depicted in Fig. 6.

Fig. 8. Densities per A-site of isolated Li-ions and Li-Li nearest-neighbor pairs in $\text{K}_{1-x}\text{Li}_x\text{TaO}_3$, as functions of x .

Fig. 9. Fourth nearest neighbor Li-Li configurations: a) ($z - z_4$); b) ($z - \bar{z}_4$), and c) ($z - x_4$).

Fig. 10. Comparison of the electronic band structures in KT40 (a), KLT40 (b), and in KLT80 with a $z - z$ Li nn-pair (c). The valence states are below zero energy.

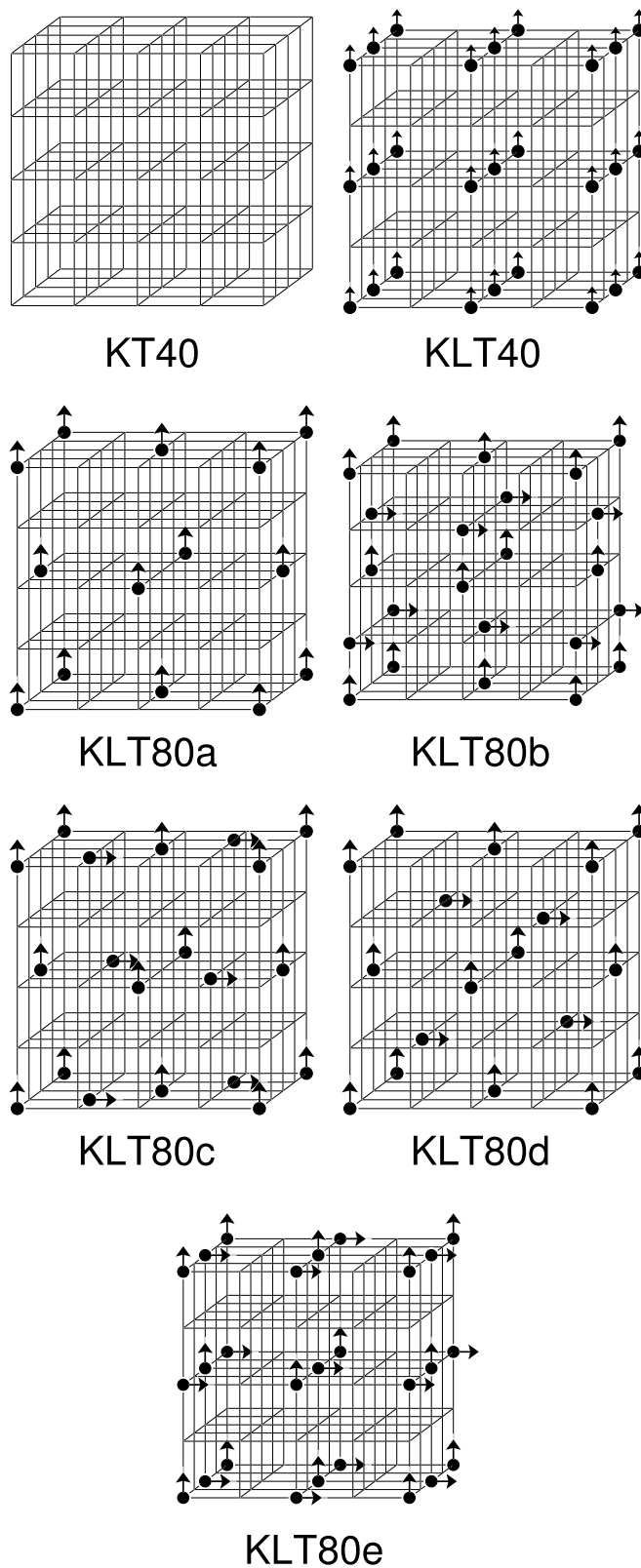


FIG. 1: Prosandeev, Cockayne, Burton, PRB

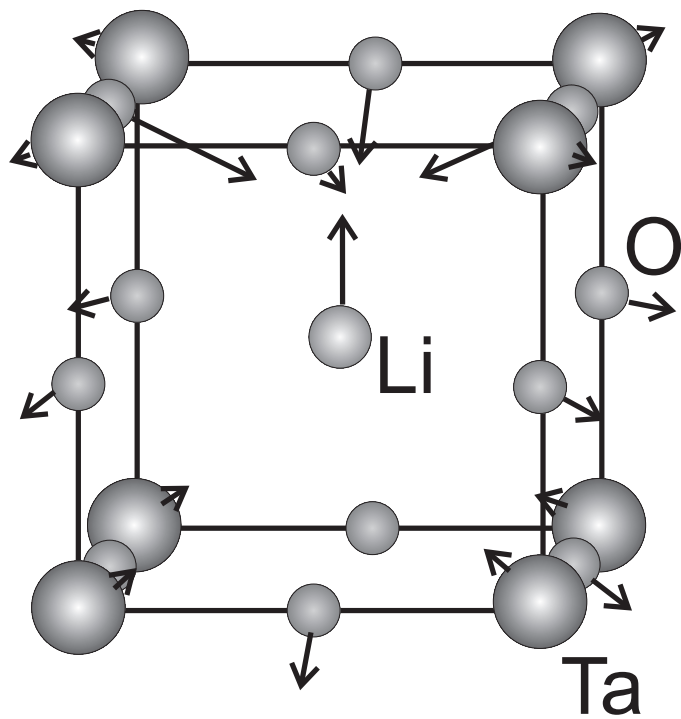


FIG. 2: Prosandeev, Cockayne, Burton, PRB

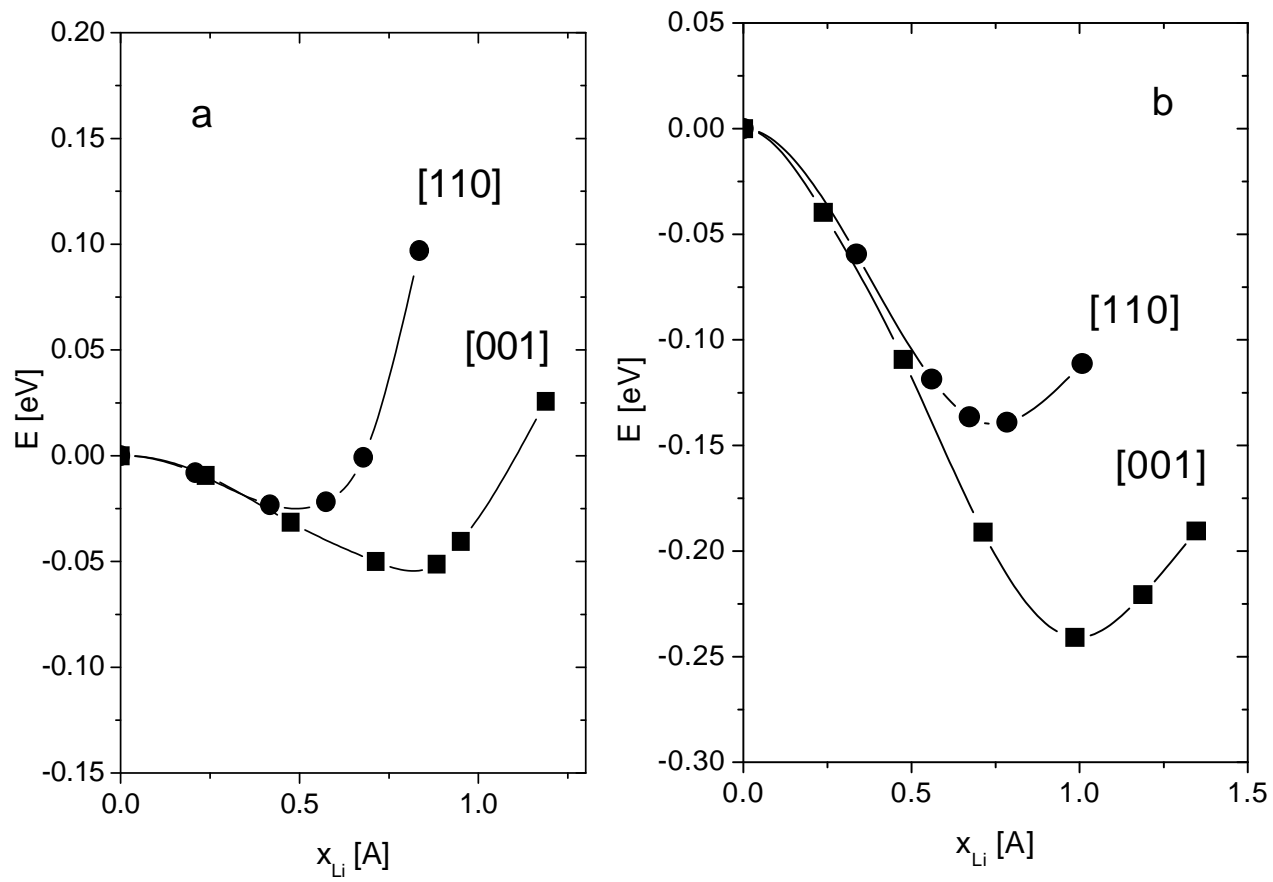


FIG. 3: Prosandeev, Cockayne, Burton, PRB

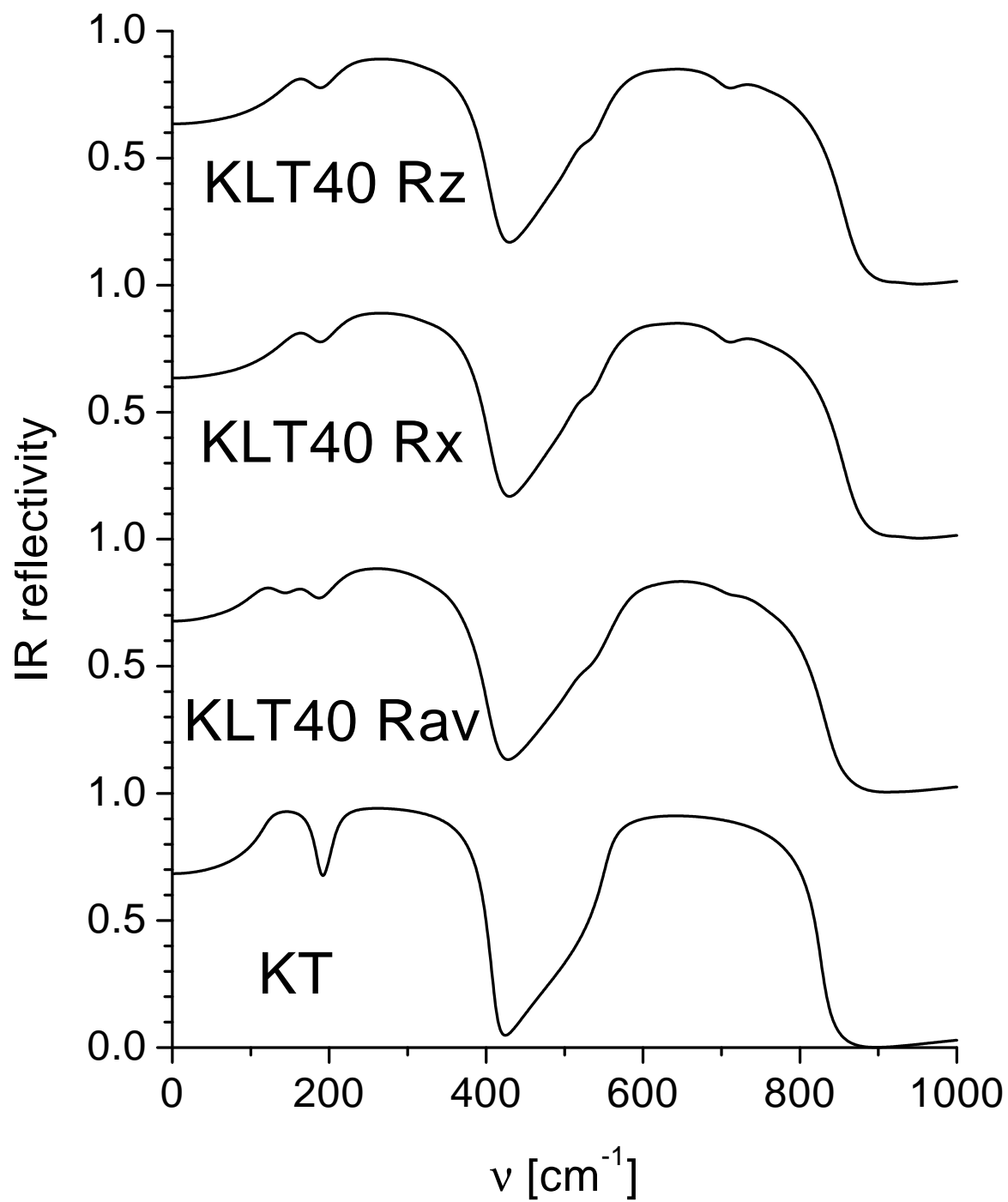


FIG. 4: Prosandeev, Cockayne, Burton, PRB

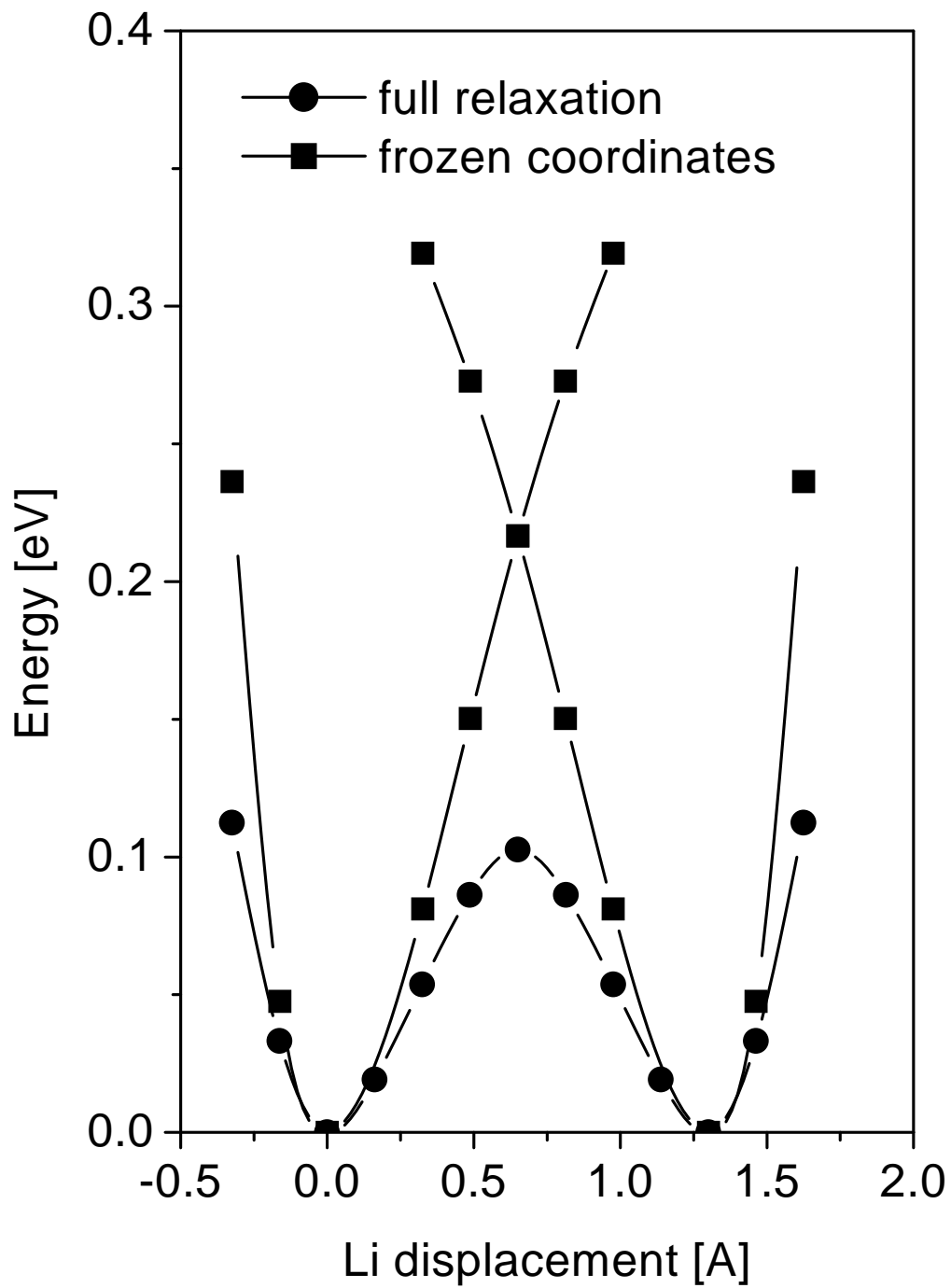


FIG. 5: Prosandeev, Cockayne, Burton, PRB

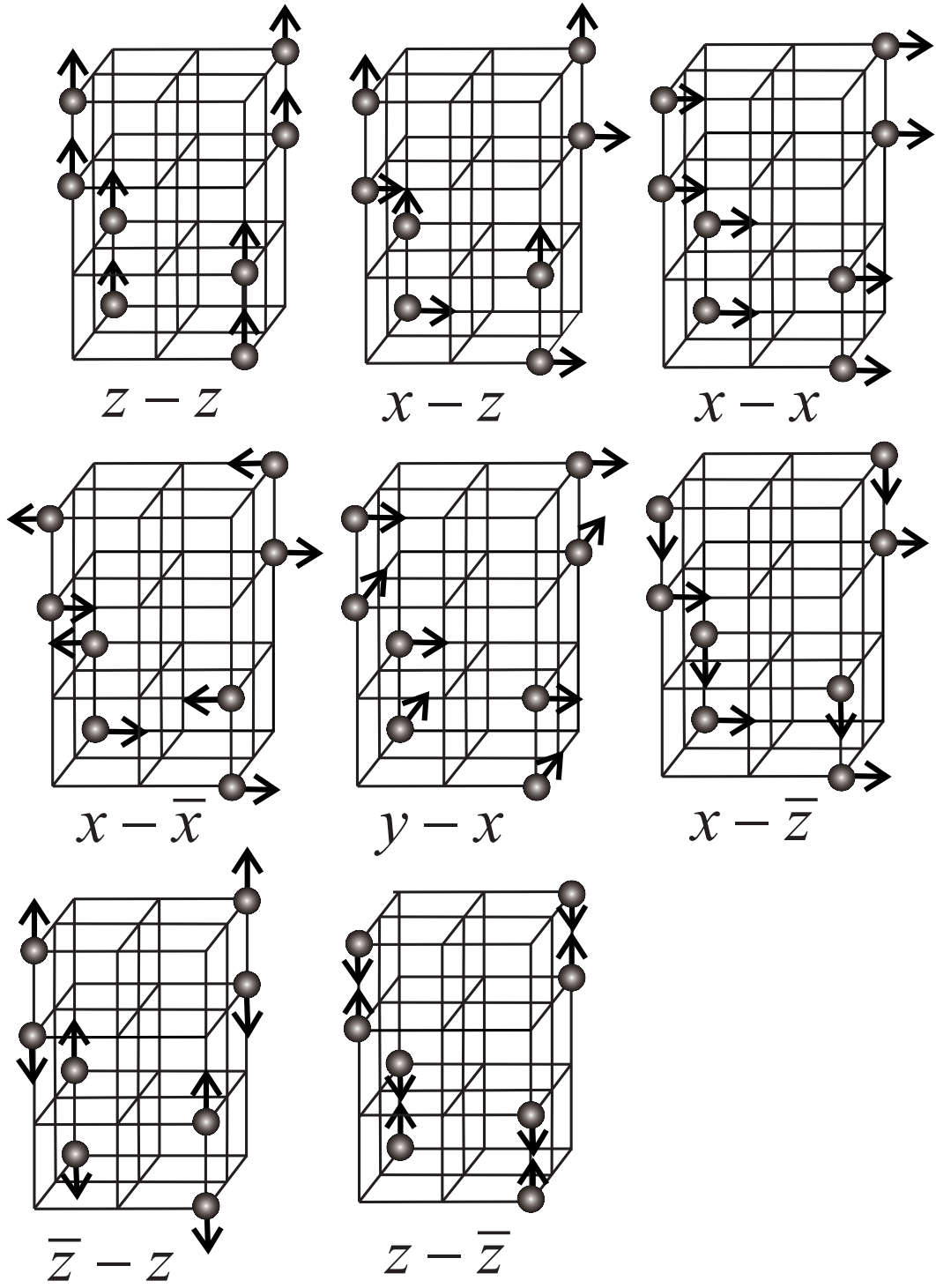


FIG. 6: Prosandeev, Cockayne, Burton, PRB

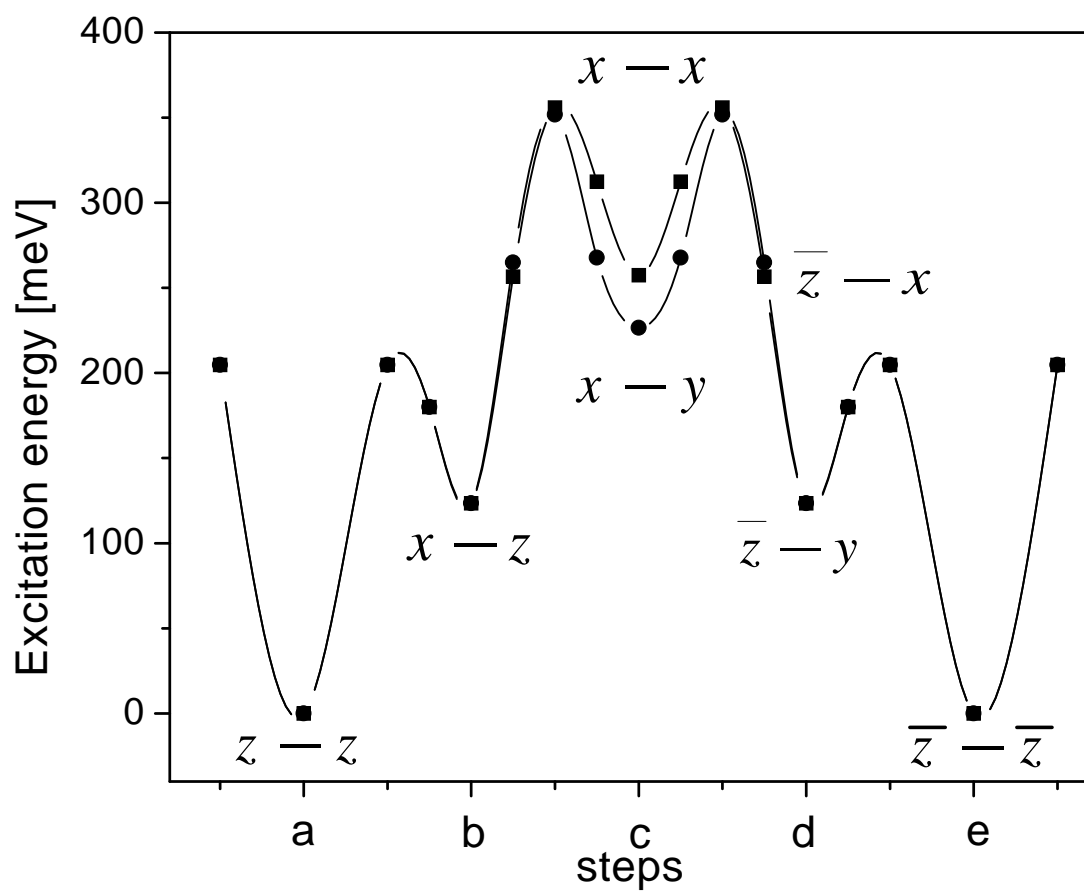


FIG. 7: Prosandeev, Cockayne, Burton, PRB

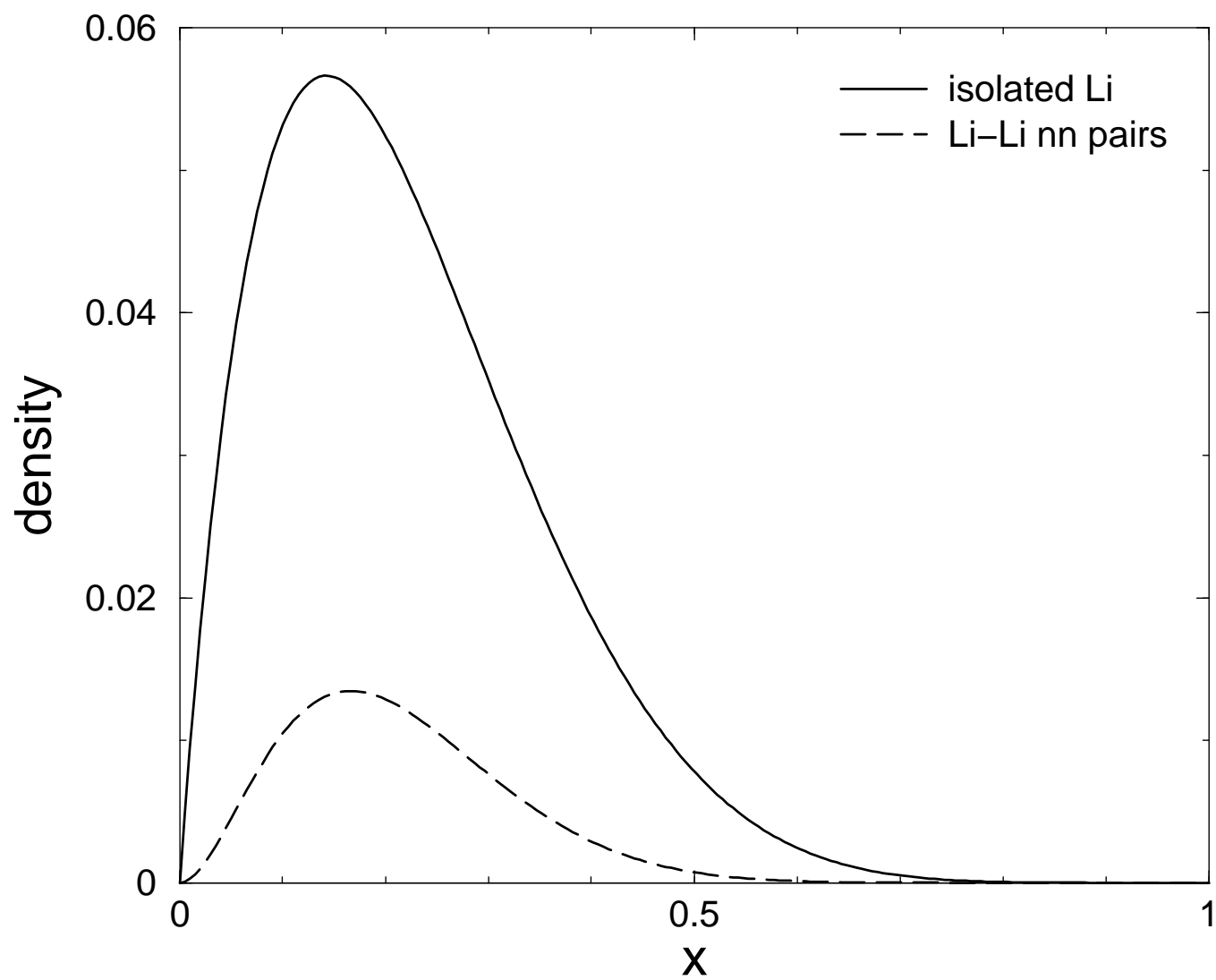


FIG. 8: Prosandeev, Cockayne, Burton, PRB

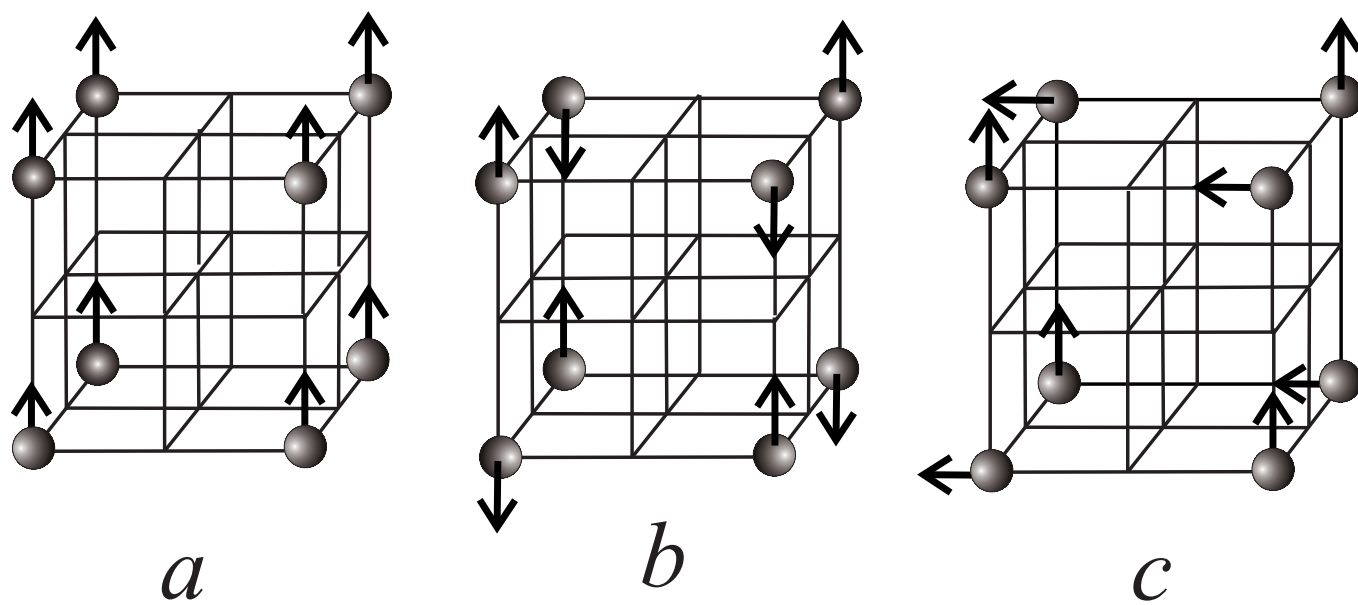


FIG. 9: Prosandeev, Cockayne, Burton, PRB

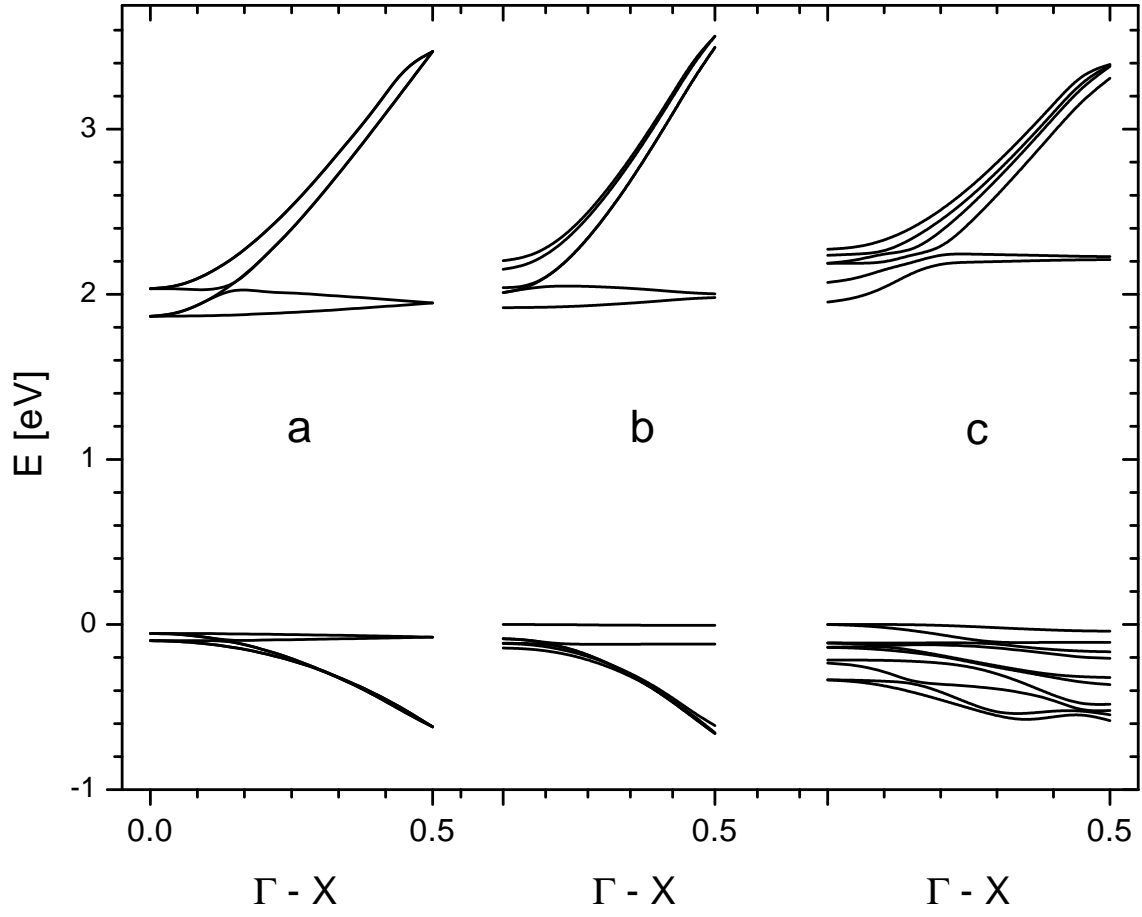


FIG. 10: Prosandeev, Cockayne, Burton, PRB